

## Heat Loads on Plasma Facing Components During Disruptions on JET

G.Arno<sup>x</sup> 1), A.Loarte 3), V.Riccardo 1), W.Fundamenski 1) A.Huber 2), and JET-EFDA contributors<sup>\*</sup>

Address: JET-EFDA, Culham Science Centre, Abingdon, OX14 3DB, UK

1) EURATOM/UKAEA Fusion Association, Culham Science Centre, Abingdon, Oxon, OX14 3DB, UK

2) Institut für Energieforschung – Plasmaphysik, Forschungszentrum Jülich, Trilateral Euregio Cluster, EURATOM-Assoziation, D-52425 Jülich, Germany

3) ITER organisation, Fusion Science and Technology Department, Cadarache, 13108 St. Paul-Lez-Durance, France

e-mail contact of main author: [gilles.arnoux@jet.uk](mailto:gilles.arnoux@jet.uk)

### Abstract:

Heat load on main chamber plasma facing component are measured with a wide angle infrared camera during disruptions on JET. For the first time, fast measurements of heat loads on the main chamber plasma facing components (about 1ms time resolution) are analysed. The timescale of energy deposition during the thermal quench is estimated and compared with timescale of the core plasma collapse measured with soft X-ray. The energy deposition time is 3-7 times longer than the plasma energy collapse during density limit disruptions or radiative limit disruptions. This factor is rather in the range 1.5-6 for vertical displacement events. The heat load profiles measured during the thermal quench show substantial broadening of the power footprint on the upper dump plate. The scrape off layer width is increased by a factor 10 for density limit disruptions and radiative limit disruptions. In the density limit disruption, the far scrape off layer is characterised by a steeper gradient by a factor 2. That could be explained by shadowing of the dump plate by other main chamber plasma facing components like the outer limiter.

---

<sup>\*</sup> See the Appendix of F.Romanelli et al. paper OV/1-2, this conference

## 1. Introduction

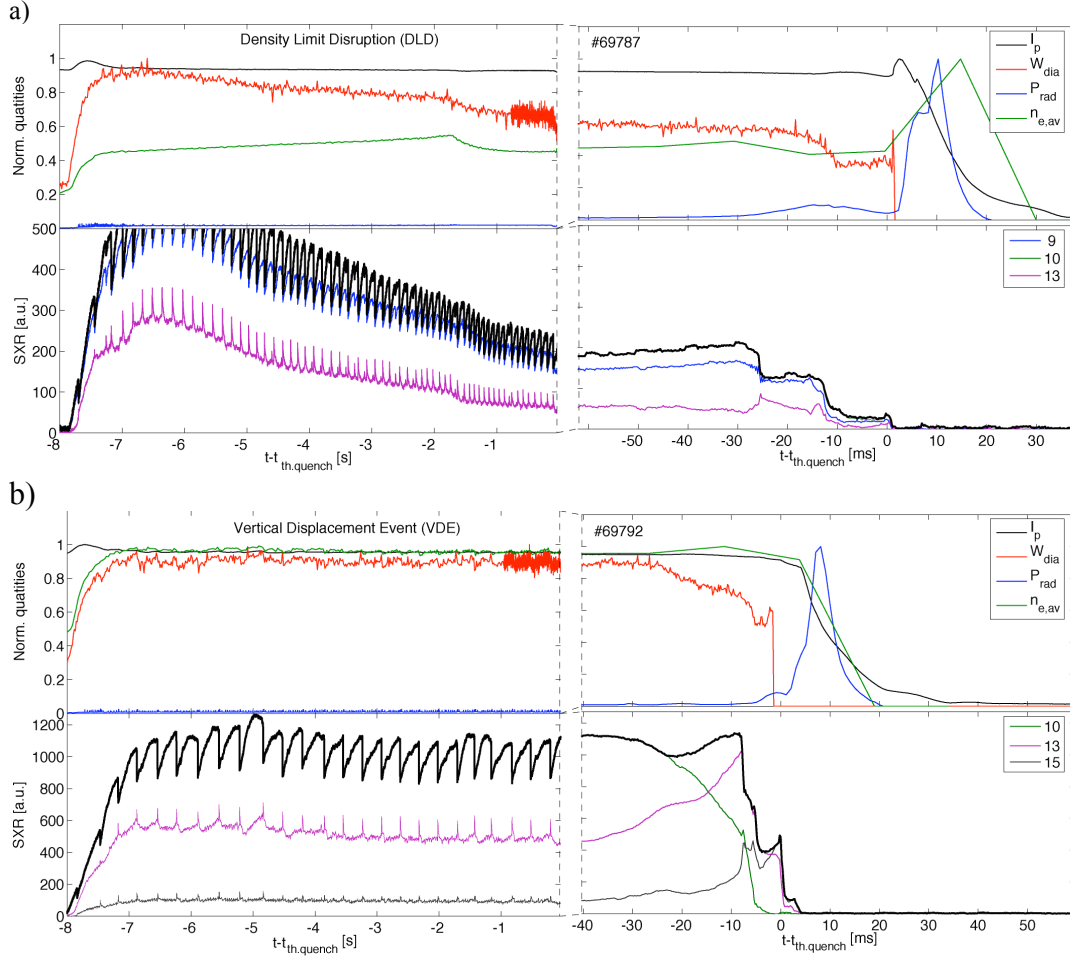


Figure 1: Normalised plasma current,  $I_p$ , diamagnetic energy,  $W_{dia}$ , total radiated power,  $P_{rad}$ , line averaged density,  $n_{e,av}$ , and absolute intensity of SXR channels (the thick line represents the maximum over all channels), for (a) a density limit disruption (DLD) and (b) a vertical displacement event (VDE). On the left, the time scale is in [s] within a time window of 8s prior to the thermal quench ( $t=0$ ). On the right, the time scale is in [ms] within a time window of 100ms around the thermal quench.

During a disruption, the thermal energy,  $W_{th}$ , is quickly lost (thermal quench) leading to a fast decrease of the plasma temperature. Consequently the plasma resistivity increases and the plasma current decays (current quench). During the thermal quench (TQ), the energy is quickly lost mainly by conduction onto the plasma facing components (PFCs). As shown in Figure 1a, in density limit disruptions (DLD) (or radiated limit disruptions (RLD)), the stored energy at the TQ is typically 25% of that at full performance plasmas. Part of the stored energy is deposited onto the divertor prior to the thermal quench on a timescale of the energy confinement time. However, at the thermal quench, a significant part of the remaining energy flows to the main chamber PFCs, in particular to the upper dump plate. This confirms recent published results [1] and is consistent with former observation [2,3], showing that between 50% and 90% of the energy is not flowing to the divertor, even in diverted configuration. During the current quench (CQ), part of the energy stored in the poloidal magnetic field,  $W_{ohmic}$ , is radiated leading to additional heat loads to the PFCs [2].

In a vertical displacement event (VDE), the control of the position is lost and the plasma moves upward on JET (see Figure 2c) resulting in limited plasma until it disrupts. When the plasma displaces upward, most of the energy is expected to flow onto the upper main chamber PFCs (upper dump plate). Because of the short warning they offer and the small fraction of stored energy that can be lost gradually before the instability, the VDEs (together with other sudden loss of confinement, like ITB collapse) are most of a concern regarding the damage to the main chamber PFCs [3].

The questions we address here are:

- 1) How quickly the energy flows onto the main chamber PFCs?
- 2) How is this energy distributed onto the main chamber PFCs?

An accurate description of the energy transfer from the plasma to the PFCs is necessary to assess the potential PFCs erosion/melting in ITER. JET is certainly the most appropriate machine to scale heat loads to ITER because of its size and its plasma stored energy.

The wide angle infrared IR camera installed in JET [4] and the recent upgrade of the bolometer systems for  $P_{rad}$  measurement [5] allow us to answer partly to the two questions above. We compare the timescales of the energy deposition (on the upper dump plate) and of the core plasma collapse during the TQ. The poloidal heat load profiles on the upper dump plate are then analysed and scrape off layer width is estimated.

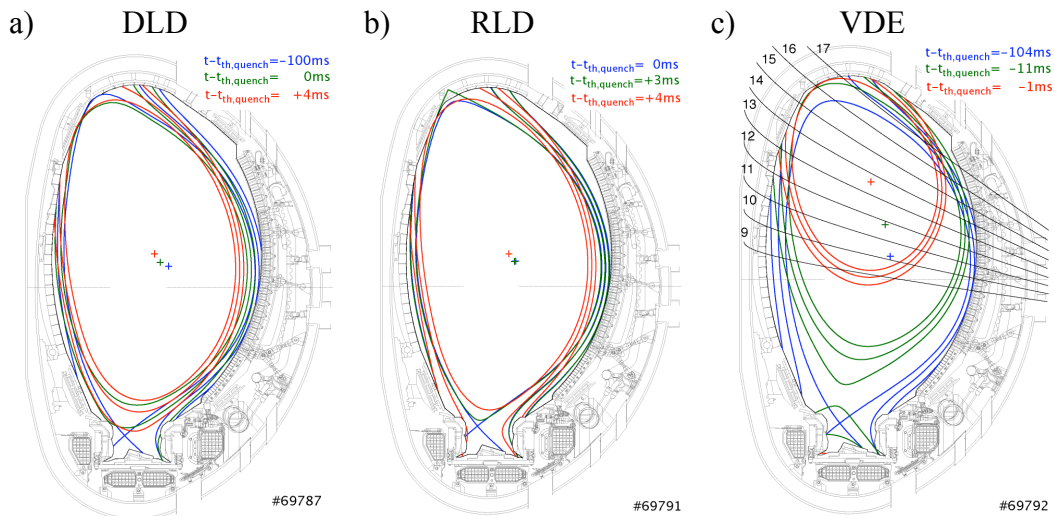


Figure 2: Magnetic equilibrium reconstruction for: (a) a density limit disruption at  $t = -100, 0$  and  $4ms$  around the TQ, (b) a radiation limit disruption at  $t = 0, 3$  and  $5ms$  after the TQ (c) a vertical displacement event at  $t = -104, -11$  and  $-1ms$  before the TQ. The magnetic surfaces are at 40 and 80 mm from the separatrix. In (c), the SXR lines of sight are superimposed.

## 2. Measurements

### 2.1. IR measurements and diagnostic issues

The heat load distribution onto the main chamber PFCs is measured with a wide angle IR camera. The IR camera provides surface temperature measurements (see examples in Figure 3a and b), and the heat loads are computed from the temperature evolution,

using the non linear finite element code THEODOR [6] (non linear here means that thermal conductivity and diffusivity depend on the temperature). 1D temperature profiles,  $T(s,t)$ , are computed from the 2D surface temperature in order to reduce the complexity of the image leading to 1D heat load profiles,  $q(s,t)$  (see sub-section 2.2 for details).

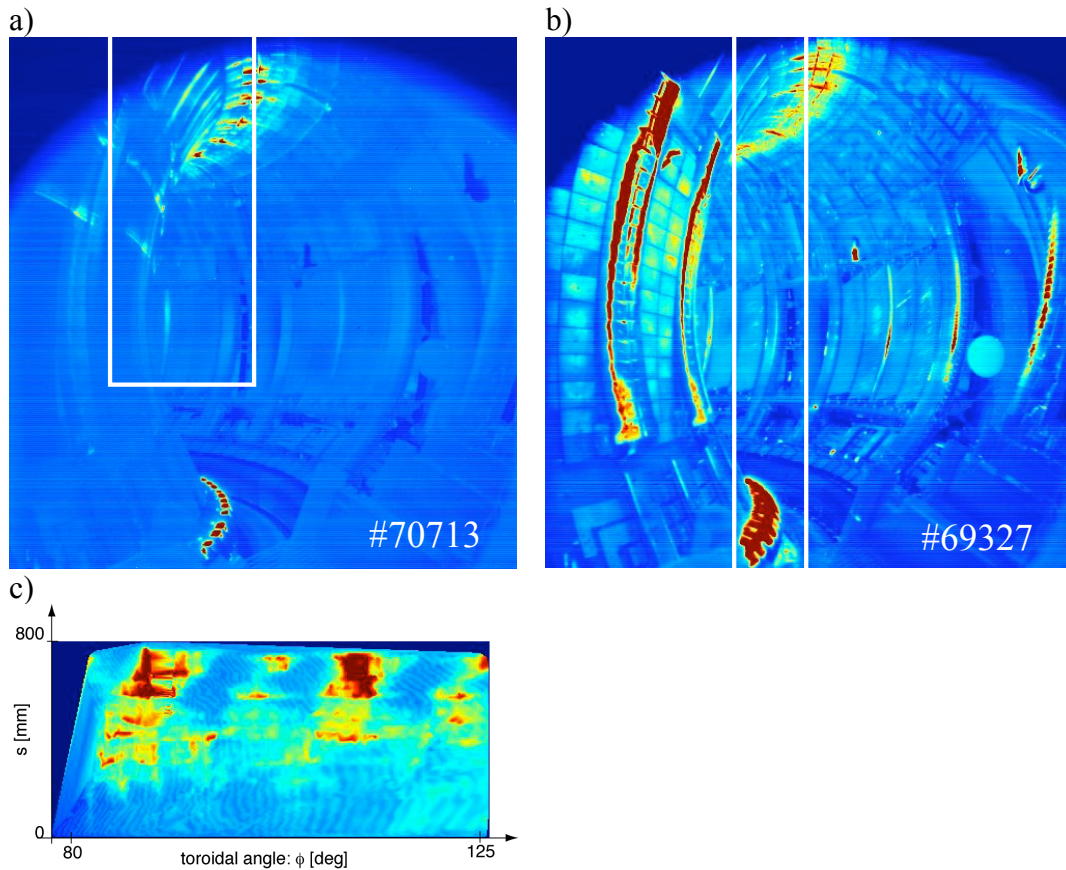


Figure 3: Images from the wide angle IR camera during a VDE (a) and a DLD (b). The white rectangles indicate the sub-windows taken for high time resolution measurements ( $1.1\text{ms} \leq \Delta t_{\text{IR}} \leq 2.3\text{ms}$ ). (c) Mapping of the upper dump plate image during a VDE (Pulse 74924). The vertical axis is the poloidal distance,  $s$ , along the upper dump plate (0 is on the high field side and 800 is on the low field side).

In our case the lateral diffusion (parallel to the surface) of the PFC is neglected since the whole disruption lasts not more than 100ms (pre-disruption phase included). The heat diffusivity of carbon fibre composite (CFC) is such that the temperature would diffuse on few mm after 100ms, which is lower than the spatial resolution of the camera (about 2cm).

In order to measure temperatures at a time resolution of the order of 1ms, the active area of the IR detector must be reduced by about an eighth of the initial image (see white rectangles in Figure 3). Such measurements can be taken only in dedicated experiments when the disruptions are purposely triggered and the camera set with optimised parameters. This has two consequences: 1) a statistical study cannot (yet) be achieved with high time resolution data, and 2) the low repetition rate of dedicated experiments on disruptions led us to make choices on the area we want to observe. The coverage of the main chamber PFCs is therefore partial. However, slow time

resolution measurements guided us in our choices. The IR data presented in section 3 have a time resolution in the range:  $1.1\text{ms} \leq \Delta t_{IR} \leq 1.8\text{ms}$

## 2.2. Heat load distribution

Figure 3a - Figure 3b illustrate the heat load distribution a few ms after the thermal quench of a VDE and of a DLD disruption respectively. The hottest parts of the PFCs are denoted by the dark red areas. These images present very complex patterns due to the many PFCs in the field of view. In the two cases of Figure 3 we observe a strong interaction with the upper dump plate (top of the image) and with the inner poloidal limiters (on the left). Note that the inner part of the divertor seems very hot but this is dominated by surface layers that heats up very quickly with not necessarily high heat loads [8]. In this paper we will concentrate our study on the upper dump plate as it is an area exposed to significant heat loads.

The complexity of the heat load footprint can be better appreciated when the image is mapped in the  $(s,\phi)$  coordinate system, where  $s$  is the distance along the dump plate in the poloidal direction (taken from the edge on the high filed side) and  $\phi$  is the toroidal angle. Figure 3c shows an example of the footprint during a VDE. In this paper, we reduce the complexity of the 2D pattern to a 1D poloidal profile by averaging the surface temperature in the toroidal direction. From the poloidal temperature profiles,  $T(s,t)$ , heat load profiles,  $q(s,t)$  are computed with a spatial resolution of  $\Delta s=60\text{mm}$  at the dump plate. This leads to underestimated heat loads but nonetheless allows us to estimate the timescale and poloidal distribution of the energy deposition.

The scrape off layer (SOL) width,  $\lambda_q$ , can be deduced from the poloidal heat load profiles. In Figure 2, we show magnetic equilibrium that can be used to map the poloidal profiles to the outer mid-plane radius,  $r$ , and calculate the associated radial power widths defined as  $\lambda_q = \int q_-(r)dr/q_{max}$ . Equilibrium reconstructions do not necessarily converge for times after the TQ, and in that case, we take the last available equilibrium.

## 2.3. Timescale of plasma collapse during the thermal quench

The measurement of the plasma collapse during the TQ is provided by the fast soft X-ray diagnostic ( $\Delta t_{SXR}=0.2\text{ms}$ ) as illustrated in Figure 1. A central and off axis channels (see Figure 2c for channel numbers) are shown, and by taking the maximum amplitude of all the channels:  $SXR_{max}$  (thick black curve), we can follow the core plasma collapse, even during a VDE where the plasma moves. The thermal quench start,  $t_{th,quench}$ , is taken at the beginning of the last crash, and in this paper all the time axis are shown relatively to  $t = t_{th,quench} = 0$ . The timescale of the energy collapse,  $\tau_{TQ,SXR}$ , is estimated by taking the decay time between 90% and 20% of the amplitude at  $t=0$ .

## 3. Results

### 3.1. Timescale of energy deposition during thermal quench

At JET the timescale of the energy collapse during the thermal quench,  $\tau_{TQ,SXR}$ , was measured to be in the range:  $1\text{ms} \leq \tau_{TQ,SXR} \leq 3\text{ms}$  [8]. Figure 4 shows a time sequence 100ms around the TQ for two different disruptions (a DLD and an RLD) and for a VDE. The main parameters ( $W_{th}$ ,  $I_p$ ,  $\tau_{TQ,SXR}$ ) and related pulse numbers are listed in

Table 0. The time scale of the energy deposition,  $\tau_{TQ,IR}$ , is estimated from the peak heat load,  $q_{pk}$ , defined as the maximum of the poloidal heat load profiles,  $q(s)$ . In the 3 cases of Figure 4,  $q_{pk}$ , reaches a first maximum quickly after  $t=0$  (TQ). We take that first peak as an indicator for the timescale of the energy deposition due to the TQ  $\tau_{TQ,IR}$ . The second peak is not relevant since it is probably dominated by radiation (it roughly corresponds with the maximum of  $P_{rad}$ ), and corresponds to the CQ phase. Figure 5a shows  $\tau_{TQ,IR}$ , as a function of  $\tau_{TQ,SXR}$  for the 5 discharges listed in Table 0. It shows that the energy deposition time is 3-7 times longer than that of the plasma collapse for DLD and RLD. For VDEs, the energy deposition seems to be rather 1.5-4 times longer. This results confirms expectations that the transport in the plasma edge plays a major role on the power flux toward the PFCs during disruptions.

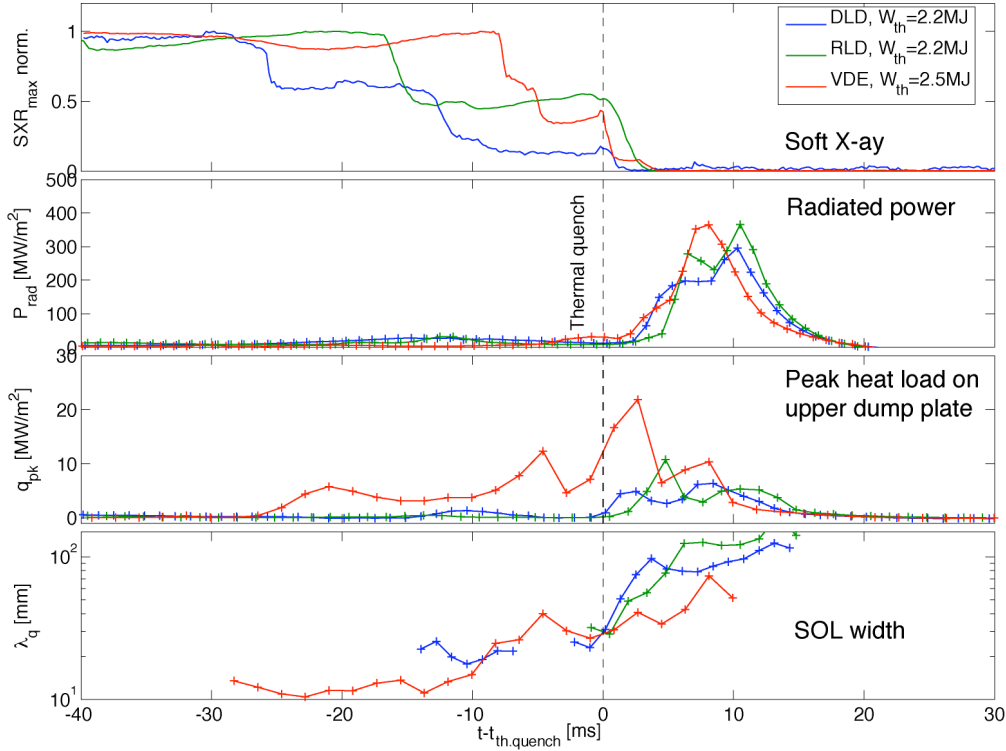


Figure 4: From top to bottom: The maximum amplitude of the Soft X-ray signal normalised, the radiated power, the peak heat load measured on the upper dump plate, and the SOL width,  $\lambda_q$ , derived from IR measurement on the upper dump plate (Note the log scale of the vertical axis). Two disruptions: a DLD (blue) and an RLD (green) are compared with a VDE (red).

### 3.2. Heat load profiles and SOL width

In this section, we analyse the heat load profiles evolution for the 3 pulses shown in Figure 4. Thanks to the high triangularity of the selected discharges, the first limited flux surface on the upper dump plate is between  $r=0-20\text{mm}$  according to the equilibrium shown in Figure 2. The SOL power width evolution,  $\lambda_q(t)$ , shown in Figure 4 (bottom) indicates a strong broadening of the profiles during the TQ for the DLD and the RLD. From  $\lambda_q=30\text{mm}$  at  $t=0$ , they increase by a factor 3-4 during the TQ (value taken after  $t=\tau_{TQ,IR}$  and before the second maximum of  $q_{pk}$ ). For the VDE, the increase is smaller (a factor 4/3), but if we take the profiles earlier, at  $t=-10\text{ms}$ , when the separatrix touches the upper dump plate, we find a smaller value:  $\lambda_q=12\text{mm}$ .

With this reference value of  $\lambda_q$ , the broadening is rather a factor 8-10 for the DLD and the RLD and a factor 3 for the VDE. These results are broadly consistent with previous observations of power load broadening on the divertor [9].

	$W_{th}$ [MJ]	$I_p$ [MA]	$\tau_{TQ,IR}$ [ms]	$\tau_{TQ,SXR}$ [ms]	$\lambda_q(t=0)$	$\lambda_q$ after TQ
69787 (DLD)	2.1	1.5	2.7	0.4	31	97 (t=3.7ms)
69791 (RLD)	2.1	1.5	5.8	1.6	29	124 (t=6.2ms)
69792 (VDE)	2.5	1.5	2.7	1.6	31	40 (t=2.7ms)
72925 (VDE)	2.8	1.5	1.6	1.0	-	-
73124 (VDE)	5.0	2.2	3.4	0.8	-	-

Table 0: List of pulses covering different type of disruptions (DLD, RLD and VDE) at various thermal energies,  $W_{th}$  and plasma current,  $I_p$ . The timescales of the energy deposition,  $\tau_{TQ,IR}$ , and of the plasma collapse,  $\tau_{TQ,SXR}$ , during the TQ, and the SOL widths at the TQ and after, are listed in the four last columns.

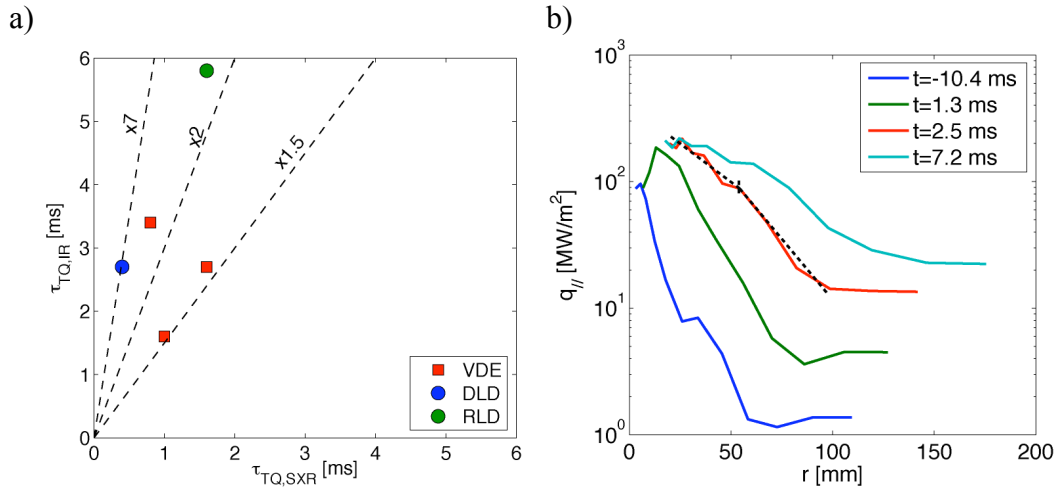


Figure 5: (a) Thermal quench timescale, determined from the heat load on the upper dump plate,  $\tau_{TQ,IR}$ , as a function of that determined from the core plasma collapse,  $\tau_{TQ,SXR}$ . (b) Parallel power flux in the SOL measured on the upper dump plate (log scale), mapped at the outer midplane radius,  $r$ , for a DLD. The power e-folding lengths,  $\lambda_{q,near}$  and  $\lambda_{q,far}$  are illustrated by the dashed line for the profile at  $t=2.5$ ms (red).

The most interesting observation can be done on the DLD profiles, where we have compute from the heat load, the power flux in the SOL parallel to the magnetic field lines,  $q_{||}$ . Four time slices of  $q_{||}$  profiles are shown in Figure 5b (log scale). At  $t=2.5$ , the profile suggests two different  $\lambda_q$ , one for the near SOL,  $\lambda_{q,near}$  ( $r < 50$ mm) and one other for the far SOL,  $\lambda_{q,far}$  ( $r > 50$ mm). The separation is indicated by the vertical marker on the profile. A linear interpolation of the 2 regions (dashed lines in Figure 5 (b)) gives the two following values:

$$\lambda_{q,near} = 33\text{mm} ; \lambda_{q,far} = 23\text{mm}$$

The lower  $\lambda_{q,far}$  indicates that the power gradient is steeper (by a factor 2.6) in the far SOL. This could be explained by the shadowing of the upper dump plate with other main chamber PFCs like the outer limiters or the divertor [10]. The magnetic equilibrium in Figure 2 (a) indicate that from  $r=80$ mm the plasma is limited by the divertor upper tiles, whereas for  $r < 80$ , the power is only shared between the upper dump plate and the inner limiter. If one refers to the wide angle IR view (pulse 69327

in Figure 3b), it seems that the interaction is rather on the outer limiters than the outer divertor. Further experiments should be carried out to confirm this result.

#### 4. Conclusion

In this paper we show the first fast measurement of heat load on the main chamber PFC during disruptions at JET. Based on the heat load measured on the upper part of main chamber, the timescale for energy deposition during the thermal quench is measured and compared with timescale for energy loss from the main plasma, measured with soft X-rays. It is found that for density limit and radiative limit disruptions the timescale for energy deposition at the upper wall during the thermal quench is substantially longer (by a factor 3-7) than the core plasma collapse time. For vertical displacement events, this ratio is smaller (a factor 1.5-4). This provides strong evidence that energy transport in the (probably) ergodised edge plasma during the thermal quench plays a major role in determining the duration of the power flux pulse.

The heat load profiles measured on the upper dump plate during the thermal quench show substantial broadening of the power footprint in agreement with previous divertor observations, with power decay length in the range 3-10cm mapped at the outer midplane radius (i.e a factor of 3-10 times larger than that for typical H-modes in these conditions). Despite this large broadening near the separatrix contact point with the upper wall, shadowing of the power fluxes to remote elements in the vacuum vessel by the JET inner wall and outer limiters leads to noticeable steeper gradient of the power flux in the far scrape off layer. This provides a guideline to be taken into account for the optimisation of the detailed design of the main wall plasma facing components in ITER.

#### References

- [1] J. Paley et al. J. Nucl. Mater., 337-339, (2005), 702-706
- [2] P. Andrew et al., J. Nucl. Mater., 363-365, (2007), 1006-1010
- [3] V. Riccardo et al., Plasma Phys. Control. Fusion, 44, (2002), 905-929
- [4] E. Gauthier et al., Proc. in 24<sup>th</sup> Symposium on Fusion Technology, Warsaw, Poland, 2006
- [5] A. Huber et al., Proc. in 34<sup>th</sup> EPS Conference on Fusion, Warsaw, Poland, 2007
- [6] A. Herrmann et al., Plasma Phys. Control. Fusion, 37, (1995), 17-29
- [7] P. Andrew et al., J. Nucl. Mater., 313-316, (2003), 135-139
- [8] V. Riccardo et al., Nucl. Fusion, 45, (2005), 1427-1438
- [9] ITER Physics Basis 1999, Nucl. Fusion, 39 2251, chapter 3
- [10] P.J. Harbour et al., Nucl Fusion, 35, (1995), 759-772

#### Acknowledgement

*This work was funded jointly by the United Kingdom Engineering and Physical Science Research Council and by the European Committee under the contract of Association between EURATOM and UKAEA. The views and opinions expressed herein do not necessarily reflect those of the European Commission.*